Available online at www.sciencedirect.com
SCIENCE DIRECT®

Journal of the European Ceramic Society 24 (2004) 2907–2915
www.elsevier.com/locate/jeurceramsoc

Probability of cone crack initiation due to spherical contact loading

V. Licht[a,*], P. Hülsmeier[a], T. Fett[b]

[a]*Universitat Karlsruhe (TH), Institut für Zuverlässigkeit von Bauteilen und Systemen, 76128 Karlsruhe, Germany*
[b]*Forschungszentrum Karlsruhe, Institut für Materialforschung II, 76021 Karlsruhe, Germany*

Received 10 July 2003; received in revised form 8 October 2003; accepted 16 October 2003

Abstract

The probability of the extension of surface cracks due to spherical indentation is analyzed. Contact loading problems typically result in multi-axle and strongly inhomogeneous stress fields near the contact surface. This property which strongly affects the stress intensity factors is taken into account in the failure analysis. Edge cracks were selected to model the actually occurring surface flaws. The stress intensity factors were integrated with the weight function method, and propagation of pre-existing cracks was assessed by using an energy release rate failure criterion. For the statistical analysis the Weibull theory was extended in some points. By applying the method to the cone crack formation during a spherical indentation, it was found that the probability for cone crack formation increases abruptly, when a certain yield load is exceeded. Therefore, the loading range can be divided into a critical and a less critical section, which were found to correlate to separated spatial regions of an occurring local risk of fracture. Because of the effects discovered, it seems to be inevitable to consider the strongly inhomogeneous stress fields in a failure analysis of a contact loading problem.
© 2003 Elsevier Ltd. All rights reserved.

Keywords: Failure analysis; Fracture; Strength; Testing; Weibull theory

1. Introduction

The consequences of a modified Weibull theory are demonstrated for the case of sphere loading. Strength of ceramic materials can be described by the Weibull distribution.[1] The interpretation of this empirically found distribution by a corresponding distribution of cracks of random size, random location, and random orientation with respect to the principal stress axes has lead to the Weibull theory of strength. Complexity of the Weibull theory increases in the following cases even in the absence of time effects (e.g. subcritical crack growth):

(a) Homogeneously distributed multiaxial stresses
(b) Complex stress states (notches), but moderate change of stresses with depth
(c) Strongly varying stresses over a length scale comparable with the crack depth
(d) Steep stress gradients with a negative mode-I stress intensity factor contribution

For crack-like defects the multiaxial theory was developed by Batdorf et al.,[2,3] Evans[4] and Matsuo.[5] The main ideas were incorporated in post-processor programs developed to evaluate the failure probability from stress computations performed by the Finite Element Method.[6,7] The Weibull theory under multiaxial, but moderately changing stresses was very often applied in literature, and some quantities (e.g. the crack density distribution) were interpreted from a special point of view. Only a few papers may be mentioned in this context.[8–12]

In some special cases, the conventional Weibull theory was not applicable. A central assumption in the derivation of basic relations is the use of a constant stress over the area of a natural crack. Deviations from this condition are obvious for sharp notches,[13] stress concentrations at bimaterial joints, contact loading with cylindrical and spherical load, and also for strongly changing stresses in thermal shock experiments.[14,15] Whereas single crack behavior has been discussed for contact loading via cylinders,[16,17] it has not yet been covered by a statistic treatment.

* Corresponding author.
E-mail address: valentin.licht@imf.fzk.de (V. Licht).

0955-2219/$ - see front matter © 2003 Elsevier Ltd. All rights reserved.
doi:10.1016/j.jeurceramsoc.2003.10.038

In the case of contact loading, cracks exhibit negative mode-I stress intensity factors. This fact and the remaining mode-II loading require the treatment of friction between crack faces. The influence considered by Alpa[18] for simple homogeneously distributed stress states has to be extended to non-homogeneous stress states.It is the aim of the present investigation to modify the conventional Weibull theory and to demonstrate the application to sphere contact loading. In particular, the location of cone-crack initiation (see e.g. Refs. 19 and 20) is computed by the fracture statistics method of 'local risk of failure'.

2. Stress field

The stress field due to spherical contact loading can be calculated for linear elastic materials in several manners.[21–23] We prefer a numerical integration based on the contact surface stress field.[21] This method has the advantage that it can also be applied to more complicated contact loading situations.

First, the stress field in a half space ($z \geqslant 0$) resulting from a concentrated point force F_0 at the surface point $(x,y,z) = (0,0,0)$ is considered. The stress field is proportional to the point force, $\sigma_{ij} = s_{ij}F_0$, and can be represented by[21]

$$s_{xx} = \frac{1}{2\pi}\left[\frac{1-2\nu}{r^2}\left\{\left(1-\frac{z}{\rho}\right)\frac{x^2-y^2}{r^2}+\frac{zy^2}{\rho^3}\right\}-\frac{3zx^2}{\rho^5}\right], \quad (1)$$

$$s_{yy} = \frac{1}{2\pi}\left[\frac{1-2\nu}{r^2}\left\{\left(1-\frac{z}{\rho}\right)\frac{x^2-y^2}{r^2}+\frac{zx^2}{\rho^3}\right\}-\frac{3zy^2}{\rho^5}\right],$$

$$s_{zz} = -\frac{3}{2\pi}\frac{z^3}{\rho^5},$$

$$s_{xy} = \frac{1}{2\pi}\left[\frac{1-2\nu}{r^2}\left\{\left(1-\frac{z}{\rho}\right)\frac{2xy}{r^2}-\frac{zyx}{\rho^3}\right\}-\frac{3xyz}{\rho^5}\right],$$

$$s_{xz} = -\frac{3}{2\pi}\frac{xz^2}{\rho^5},$$

$$s_{yz} = -\frac{3}{2\pi}\frac{yz^2}{\rho^5},$$

with $r = \sqrt{x^2+y^2}$ and $\rho = \sqrt{x^2+y^2+z^2}$. This solution can be taken as a Green function to integrate the stress field inside the half space under quite general boundary conditions.

Next, a sphere with radius R is assumed to be pressed onto the half space with the force F. A circular contact region results, with the pressure distribution[21,24]

$$p(x,y) = \begin{cases} \dfrac{3F}{2\pi r_c^2}\sqrt{1-\dfrac{x^2+y^2}{r_c^2}} & \text{for} \quad \sqrt{x^2+y^2} \leqslant r_c \\ 0 & \text{for} \quad \sqrt{x^2+y^2} > r_c \end{cases} \quad (2)$$

The contact radius r_c is determined by

$$r_c = \left(\frac{3FR}{4E'}\right)^{1/3}, \quad (3)$$

with E' being the reduced Young's modulus

$$E' = \left(\frac{1-\nu_1^2}{E_1}+\frac{1-\nu_2^2}{E_2}\right)^{-1}, \quad (4)$$

and $E_{1/2}$ and $\nu_{1/2}$ the elastic parameters of the sphere and the half space, respectively.

Finally, the stress field inside the half space due to spherical contact loading is found to be

$$\sigma_{ij}(x,y,z) = \int_A p(x',y')s_{ij}(x-x',y-y',z)dx'dy', \quad (5)$$

with the integration spreading over the surface of the half space. This integral can be evaluated numerically.

Contact loading is centered at $x = y = 0$ by definition, so that the system is axisymmetric around the z-axis. Therefore, it is sufficient to restrict all considerations to the xz-plane, where σ_{xx} and σ_{yy} can be identified as the radial and angular stress components, respectively, and σ_{xy} and σ_{yz} vanish due to the symmetry.

An example of an indentation with a force of $F = 50$ N is given in Fig. 1 (see Table 1 for the elastic parameters and the geometry). It is obvious that the stress components have very high gradients near the contact region. The radial stress component in particular changes rapidly from a maximum tension at the surface to pressure deeper inside the material. The shear stress vanishes at the surface, but then increases very fast below.

3. Selection of crack type

Natural cracks at the surface of ceramic test specimens are mostly modeled as semi-circular cracks in a

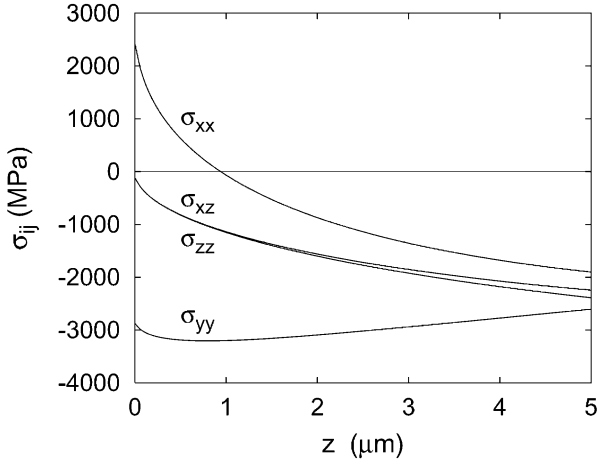

Fig. 1. Stress field components along z direction at $x = r_c$.

Table 1
Material parameter and geometry

Material	Curvature R (mm)	Young's modulus E (GPa)	Poisson's ratio ν
Diamond	0.5	1050	0.17
Al_2O_3	∞	380	0.22

half space. During load application, the initial shape may change, resulting in a semi-elliptical crack. Such a crack of depth a and width $2c$ is illustrated in Fig. 2a. The loading situation is characterized sufficiently by the stress intensity factors at the deepest point (A) and the surface points (B) of the semi-ellipse. Different methods may be applied for the computation of the related stress intensity factors K_A and K_B. For our computations the stress distribution σ_{xx} of Fig. 1 was fitted by a polynomial

$$\sigma(z) = \sum_{n=0}^{4} C_n z^n \tag{6}$$

providing the five coefficients $C_0 \ldots C_4$. The stress intensity factors are then given by[25]

$$K_{A,B} = \sqrt{a} \sum_{n=0}^{4} C_n Y_{(n)A,B} a^n \tag{7}$$

with the geometric functions $Y_{(n)A,B}$ tabulated in Ref. 25 for $0 \leqslant a/c \leqslant 1$. By application of cubic splines, the tabulated data were interpolated. In Fig. 2b the two stress intensity factors are shown for a sphere loading of $F = 75$ N as a function of a and a/c.

The evolution of a half-penny-shaped surface crack under sphere loading can be concluded from Fig. 3. An initial crack of depth $a_0 = 1$ μm is assumed to exist at $x = r_c$. For this crack the stress intensity factor K_B is higher than K_A by a factor of about 5. Under increasing load, the crack must first extend in c-direction, since $K_B = K_{Ic}$ is reached at a load, at which K_A is clearly smaller than K_{Ic}. Extension in c-direction leads to a decrease in a/c and, consequently, in K_B. K_A simultaneously increases. At a critical aspect ratio of $(a/c)_c = 0.15$, both stress intensity factors become identical (solid circle in Fig. 3a). Now, the crack may also extend in the direction of depth. The related result is introduced in Fig. 3b, where the critical aspect ratio is plotted versus the initial crack depth a_0.

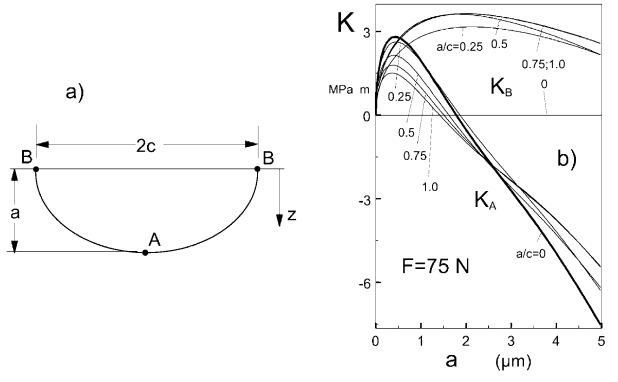

Fig. 2. Semi-elliptical surface crack, (a) geometric data, (b) stress intensity factor K_A at the deepest point and K_B at the surface points for a load of $F = 75$ N.

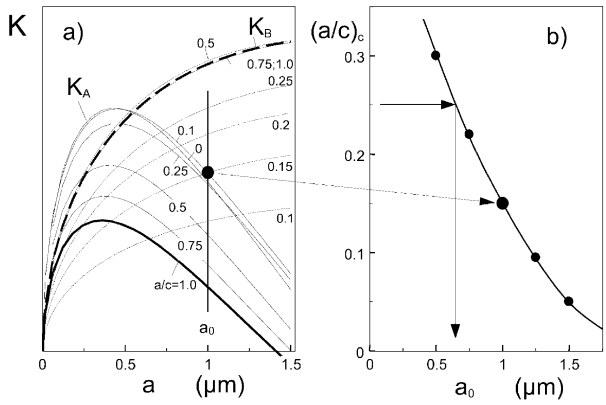

Fig. 3. (a) Determination of the critical aspect ratio at the beginning of crack growth in depth direction for an initial crack depth of $a_0 = 1$ μm, (b) critical aspect ratio as a function of the initial crack depth.

As can be seen from the K_A-curves in Fig. 3a, the stress intensity factor at the deepest point of a semi-ellipse is identical with that of the edge crack ($a/c = 0$) within a deviation range of 10%, if $a/c < 0.25$. In our example this is the case for $a_0 \geqslant 0.65$ μm (see arrows in Fig. 3b). Under this condition, the edge-crack stress intensity factor solution can be applied as a good approximation. Therefore, the edge-crack solution is used for our further computations of K_A.

The authors are aware of the fact that for modelling the ring crack formation under increasing load, use of the full stress intensity factor solution as a function of a and a/c is necessary.

4. Effective stress intensity factors

The surface cracks are initiated at naturally existing flaws or small cracks which may be induced by manufacturing. To model such flaws, surface cracks with an arbitrary orientation are assumed (Fig. 4).

Usually, the stress is assumed to be nearly constant in the range of the natural flaws. This allows for the calculation of the K factors with the help of simple functions depending on the crack length and stress. But as we have seen above, this assumption fails for contact loadings. The stress can also change remarkably on small scales. The stress intensity factor must then be integrated along the crack length a by applying the weight function method.[25] As an approximation for the mode-I and mode-II stress intensity factors we use

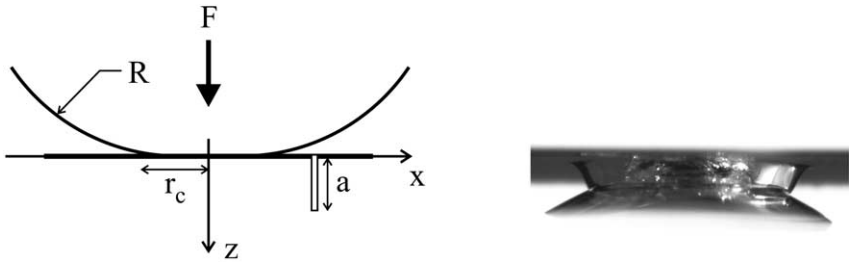

Fig. 4. Left: Spherical contact loading with a tangentially oriented edge crack near the contact boundary. Right: Side view of a cone crack in glass.

$$K_I(a) = \int_0^a \sigma(z) h_I(z, a) dz, \tag{8}$$

$$K_{II}(a) = \int_0^a \tau(z) h_{II}(z, a) dz, \tag{9}$$

where σ and τ are the normal and shear stress, respectively. The weight functions are equal for the edge-cracked half-space, $h_I = h_{II} = h$, and can be approximated by

$$h(z, a) = \sqrt{\frac{2}{\pi a}} \sum_{n=0}^{6} D_n \left(1 - \frac{z}{a}\right)^{n-\frac{1}{2}}. \tag{10}$$

The coefficients are found to be[25]

$$\begin{aligned} D_0 &= 1.0, \\ D_1 &= 0.58852, \\ D_2 &= 0.031854, \\ D_3 &= 0.463397, \\ D_4 &= 0.227211, \\ D_5 &= -0.828528, \\ D_6 &= 0.351383. \end{aligned} \tag{11}$$

If the orientation of the crack is determined by the crack-plane-normal vector

$$(n_i) = (\cos\varphi, \sin\varphi, 0), \tag{12}$$

the normal and shear stresses are given by

$$\sigma(z) = \sigma_{xx}(z)\cos^2\varphi + \sigma_{yy}(z)\sin^2\varphi, \tag{13}$$

$$\tau(z) = \sigma_{xz}(z)\cos\varphi. \tag{14}$$

Because of the strong shear stresses near the contact region, we consider a failure of cracks under a mixed mode loading. As failure criterion, the energy release rate criterion was selected,[16] where both, K_I and K_{II}, contribute to the effective stress intensity factor. The effective stress intensity factor is defined as[29,30]

$$K_{eff} = \begin{cases} \sqrt{K_I^2 + K_{II}^2} & \text{for } K_I \geqslant 0 \\ \mu K_I + |K_{II}| & \text{for } K_I < 0 \end{cases}. \tag{15}$$

Hereinafter, the friction coefficient μ is chosen to be 0.5 (Table 2).

The stress intensity factors of a tangentially oriented edge crack, $\varphi = 0$, at the contact boundary, $x = r_c$, are shown in Fig. 5. A contact loading of $F = 50$ N is assumed as above. K_I is positive for small z, but then becomes negative, because of the rapidly decreasing radial stress component. K_{II} is of the same order as K_I, but vanishes at the surface. Near the surface, the resulting effective stress intensity factor is dominated by K_I. A slight kink occurs in the K_{eff} curve, when K_I

Table 2
Fracture mechanics coefficients of the Al_2O_3 ceramics considered

Fracture toughness	K_{Ic}	3.95 MPa $m^{1/2}$
Weibull parameter	σ_0	525.6 MPa
Weibull exponent	m	10.3
Friction coefficient	μ	0.5

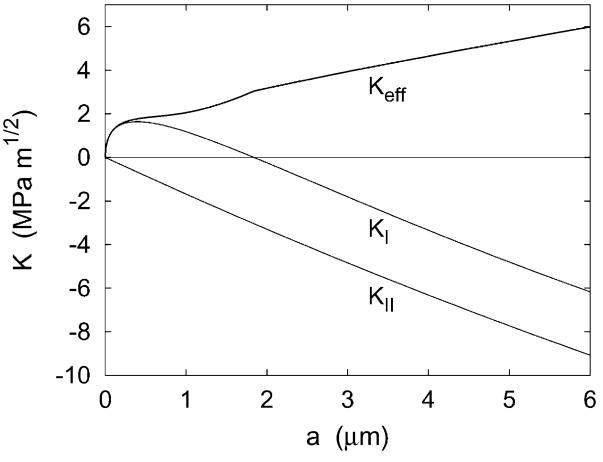

Fig. 5. Stress intensity factors of a tangentially oriented edge crack at $x = r_c$.

changes its sign. Behind this point, further increase of the effective stress intensity factor is dominated by K_{II}.

5. Critical crack lengths

For a material with an effective fracture toughness K_{Ic}, it is assumed that all crack lengths of

$$K_{eff}(a) \geqslant K_{Ic} \tag{16}$$

are critical. Fig. 6 shows an example of the loading case discussed before with the fracture toughness given in Table 2. The total set of critical crack lengths A_c is found to be

$$A_c = [a_1, a_2] \cup [a_3, \infty]. \tag{17}$$

To be more accurate, the history of the loading process also has to be taken into account, as a crack, which was critical once keeps this attribute. In general, the set of critical crack lengths at the time t can be defined as

$$A_c = \{a | \exists \tau \leqslant t : K_{eff}(a, \tau) \geqslant K_{Ic}\}. \tag{18}$$

It is self-evident that A_c depends on the location and orientation of the cracks in each case.

This definition of critical crack length allows to decide, whether a crack is able to grow or remains unaltered. From Fig. 6, it might erroneously be concluded that for this loading state, cracks of size $a_1 \leqslant a < a_2$ would stop at $a = a_2$, because the actual stress intensity factor then falls below K_{Ic}. The considerations made before do not provide any information on further crack growth phases, since the computations were based on the assumption of a coplanar crack extension. In the situation described before, the cracks are under mixed-mode loading. Therefore, crack kinking must be taken into account. If such a crack starts to propagate, e.g. at an initial crack depth a_1, the crack abruptly changes its direction by generating a kink and then satisfies $K_{II} = 0$.

The kink behavior is illustrated in Fig. 7 for different initial crack depths a_1, a_2, and a_3. For these crack sizes, the condition $K_{eff} = K_{Ic}$ may be fulfilled (Fig. 7a). From the stress intensity factor computations, we find e.g. for a crack of depth a_2 that the ratio of the mode-II and mode-I stress intensity factors is $|K_{II}|/K_I \approx 0.5$ (Fig. 7b). In Fig. 7c the kink angle β is plotted for the criterion of maximum K_I at the tip of the kinked crack as a function of mode mixity.[26] It should be noted that for any mixed-mode criterion, the relation $\beta = f(K_{II}/K_I)$is nearly identical. In Fig. 7d, the kinked crack is shown. For $a < 3$ μm, the mode-II stress intensity factor contribution is negligible and, consequently, crack deflection is not possible. Such small cracks extend in the initial crack direction.

For crack size a_3, a mode-I stress intensity factor contribution does not exist. Consequently, the kink angle becomes maximum (i.e. $\beta = 76°$).

As outlined before, crack kinking is governed by the condition of maximum K_I or, equivalently, by $K_{II} = 0$. For longer crack extension after kinking, this condition is fulfilled for a crack shape coinciding with the so-called cone crack (Fig. 4), which is roughly in agreement with the maximum principal stress trajectory.[27,28] Such considerations are not an adequate tool to consider failure statistics.

Therefore, the consideration below is restricted to the question of where the formation of a cone crack has to be expected (Fig. 4).

In this sense, 'failure' is defined independently of whether there is only an increase in length, followed by crack arrest (as occurring under sphere loading by formation of cone cracks) or whether total failure may occur by unstable crack propagation (occurring under cylinder loading)—as the first extension in depth direction.

For the formation of a ring-shaped crack, a single crack must not necessarily extend in circumferential direction until a closed ring is reached. At any location along the circumference, the probability of crack growth

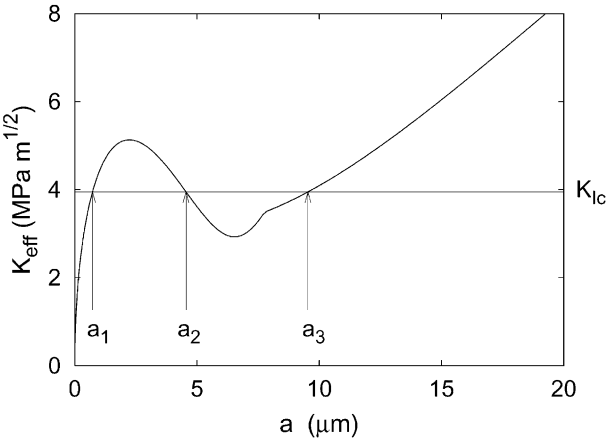

Fig. 6. Stress intensity factor of tangentially oriented edge cracks at $x = 1.15\ r_c$. The loading force is $F = 100$ N.

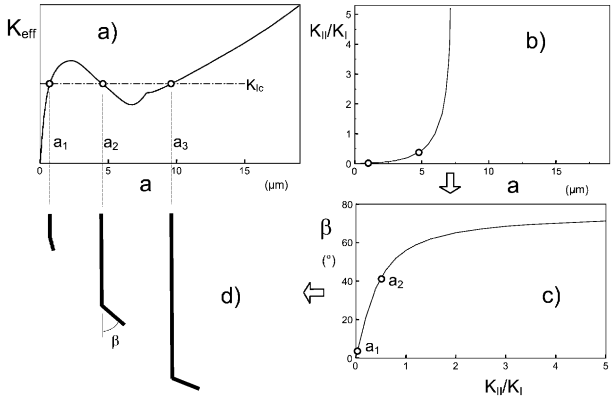

Fig. 7. Crack extension and crack deflection for cracks of different size.

in width and depth direction is the same (i.e. the local risk of crack extension is independent of the circumference angle). Consequently, coalescence of a number of individual cracks results in a ring crack. This means that crack extension is not a local effect, but occurs around the sphere with same probability.

6. Extended Weibull theory

As mentioned in the introduction, the conventional Weibull theory uses the approximation of nearly constant stress along natural flaws. Thus, simple relations for the stress intensity factor are found, which can be incorporated in the theory. In our example of application to single cracks, it becomes obvious that considerations of statistically distributed natural cracks, based on the commonly used Weibull theory, must fail. The main reasons are:

- Inhomogeneous stresses with strong gradients, and
- strongly multi-axial stress states with a change of multiaxiality over dimensions in the order of the crack length.
- Moreover, also friction effects between crack faces under negative mode-II stress intensity factor contributions have to be taken into account.

These reasons make an extension of the commonly used formulation of the Weibull theory necessary. As an application of the modified Weibull formulation, we try to compute the radius of the cone crack at the specimen surface and the load when cone crack initiation has to be expected.

6.1. Failure probability

In the probabilistic theory, a single crack is characterized by its length a, its location x,y, and its orientation φ. Lacking the entire information about the cracks, these quantities are treated as independent random variables. Assuming homogeneous and isotropic properties, the distribution densities of the location and orientation are $f_{x,y}(x,y) = 1/A$ and $f_\varphi(\varphi) = 1/(2\pi)$, with A being the surface area of the component considered. A cumulative Pareto distribution is assumed to apply to the crack length[2]

$$F_a(a) = \begin{cases} 1 - \left(\dfrac{\bar{a}_0}{a}\right)^{m/2} & \text{for } a > \bar{a}_0 \\ 0 & \text{else,} \end{cases} \tag{19}$$

with the parameters $\bar{a}_0$ and m. The corresponding density function is found to be $f_a(a) = dF_a(a)/da$.

If the set of critical crack lengths is given by $A_c(x,y,\varphi)$, the failure probability for a component with one flaw is

$$\begin{aligned} P_F^{(1)} &= \int_S \int_\Omega \int_{A_c(x,y,\varphi)} f_{x,y}(x,y) f_\varphi(\varphi) f_a(a) da d\varphi dx dy \\ &= \frac{1}{2\pi A} \int_S \int_\Omega \int_{A_c(x,y,\varphi)} f_a(a) da d\varphi dx dy, \end{aligned} \tag{20}$$

where S denotes the surface of the component and $\Omega = [0, 2\pi]$ the range of crack orientation.

In the presence of more than one crack, the 'weakest link' hypothesis is valid. For n cracks, we therefore find a failure probability of $P_F^{(n)} = 1 - \left(1 - P_F^{(1)}\right)^n$. As the actual number of cracks is unknown, a Poisson distribution of $p_n = e^{-M} M^n/n!$ is assumed for the crack number with a mean value of M. The probability of a component containing exactly n cracks and failing is then found to be $p_n P_F^{(n)}$. When summing up this expression over all possible values of n, the mean failure probability of

$$P_F = 1 - \exp\left(-M P_F^{(1)}\right) \tag{21}$$

is obtained.

For cracks with orientation φ located at x,y, a general set of critical crack lengths is assumed

$$A_c = [a_1, a_2] \cup \ldots \cup [a_r, \infty], \tag{22}$$

where the quantities $a_1 \ldots a_r$ are the roots of $K_{eff}(a) = K_{Ic}$. With the help of the cumulative Pareto distribution (19) the failure probability in case of one flaw (20) can then be partially integrated

$$P_F^{(1)} = \frac{1}{2\pi A} \int_S \int_\Omega \sum_{i=1}^{r} (-1)^{i+1} \left(\frac{\bar{a}_0}{a_i(x,y,\varphi)}\right)^{m/2} d\varphi dx dy. \tag{23}$$

Inserting this in (21) the mean failure probability is found to be

$$P_F = 1 - \exp\left(-\frac{1}{2\pi A_0} \int_S \int_\Omega \sum_{i=1}^{r} (-1)^{i+1} \left(\frac{a_0}{a_i(x,y,\varphi)}\right)^{m/2} d\varphi dx dy\right), \tag{24}$$

where the unit area A_0 and the parameter $a_0 = \bar{a}_0 A_0^{2/m} (M/A)^{2/m}$ have been introduced.

By comparison with the conventional Weibull theory, m turns out to be the Weibull exponent. The parameter a_0 is related to the Weibull parameter σ_0 of a conventional strength test under sufficiently constant stresses (e.g. bending strength test) determined by

$$a_0 = \left(\frac{K_{Ic}}{Y_I \sigma_0}\right)^2, \tag{25}$$

with $Y_I = 1.98$ for the cracks in the strength test modelled by edge cracks or $Y_I = 1.3$ for semi-circular surface cracks.

6.2. Local risk of fracture

A useful quantity for the interpretation of the spatial failure distribution is the local risk of fracture $p_F(x,y)$, which is a density function in contrast to the cumulative failure probability P_F. On condition that a component fails due to one flaw, $p_F(x,y)dxdy$ determines the probability of the failure occurring in the surface element $dxdy$ at the point x,y. Eqs. (19) and (20) yield

$$p_F(x,y) = \frac{\int_\Omega \int_{A_c(x,y,\varphi)} f_a(a) da d\varphi}{\int_S \int_\Omega \int_{A_c(x,y,\varphi)} f_a(a) da d\varphi dx dy} = \frac{\int_\Omega \sum_{i=1}^{r} (-1)^{i+1} a_i(x,y,\varphi)^{-m/2} d\varphi}{\int_S \int_\Omega \sum_{i=1}^{r} (-1)^{i+1} a_i(x,y,\varphi)^{-m/2} d\varphi dx dy}. \quad (26)$$

For the axisymmetric contact problem, the local risk is a function of the radius only, $p_F(x,y) = p_F(r(x,y))$. Therefore, it is common practice to integrate $p_F(r)$ over $rd\vartheta$ and to define the quantity

$$p_F^*(r) = \int_0^{2\pi} p_F(r) r d\vartheta = 2\pi r p_F(r) \quad (27)$$

which is the local risk in terms of the radius.

6.3. Accuracy of numerical evaluation

Any numerical analysis of the set of critical crack lengths must be cut off in practice at a certain maximum crack length $a_{\max}$. Therefore, failure probability can be determined only with a limited accuracy which will be estimated below.

The set of critical crack lengths can be expressed as the sum $A_c = A'_c + A''_c$ of the subsets

$$A'_c = A_c \cap [0, a_{\max}] \quad (28)$$

$$A''_c = A_c \cap (a_{\max}, \infty).$$

Only A'_c can be analyzed in practice.

Using these subsets, the failure probability in the case of one crack is equal to $P_F^{(1)} = P_F^{'(1)} + P_F^{''(1)}$, where $P_F^{'(1)}$ and $P_F^{''(1)}$ are defined by Eq. (20), with the integration restricted to A'_c and A''_c, respectively. The mean failure probability (21) can then be rewritten as

$$P_F = 1 - \exp\left(-MP_F^{'(1)} - MP_F^{''(1)}\right). \quad (29)$$

The actually evaluated probability, denoted by P'_F, will underestimate this value

$$P'_F = 1 - \exp\left(-MP_F^{'(1)}\right) \leqslant P_F. \quad (30)$$

The difference is found to be

$$\Delta P_F = P_F - P'_F = \exp\left(-MP_F^{'(1)}\right)\left[1 - \exp\left(-MP_F^{''(1)}\right)\right] \leqslant 1 - \exp\left(-MP_F^{''(1)}\right). \quad (31)$$

To obtain an applicable estimation, the exponential term is reduced. As we know that $A''_c \subset (a_{\max}, \infty)$, it can be derived that

$$\exp\left(-MP_F^{''(1)}\right) \geqslant \exp\left(-\frac{M}{2\pi A}\int_S\int_\Omega\int_{a_{\max}}^{\infty} f_a(a) da d\varphi dx dy\right) = \exp\left(-\frac{A}{A_0}\left(\frac{a_0}{a_{\max}}\right)^{m/2}\right), \quad (32)$$

into which Eq. (19) and the definition of the parameter a_0 have been inserted. With this result, we are finally able to give an upper limit for the error of the failure probability

$$\Delta P_F \leqslant 1 - \exp\left(-\frac{A}{A_0}\left(\frac{a_0}{a_{\max}}\right)^{m/2}\right) \approx \frac{A}{A_0}\left(\frac{a_0}{a_{\max}}\right)^{m/2}, \quad (33)$$

where the approximation holds for sufficiently large $a_{\max}$. This relation can also be used to choose a proper value of $a_{\max}$, if a certain accuracy shall be maintained in a numerical analysis.

7. Results

The modified Weibull theory was applied for the analysis of spherical contact loading. The contact problem considered was defined by the material parameters and fracture mechanics coefficients listed in Tables 1 and 2, respectively. The history of the loading process, whose influence on the set of critical crack lengths was pointed out in Section 5, was neglected in the calculations. Therefore, there may be some deviations from a history-dependent analysis, but it is assumed that these effects are small in our case and that the characteristics of the results are unaltered.

The evaluated probability of surface crack initiation is shown as a function of the applied load in Fig. 8. The evolution of the probability is divided into two sections. At first, there is a moderate increase of the probability with comparable low values. But then, at a critical load

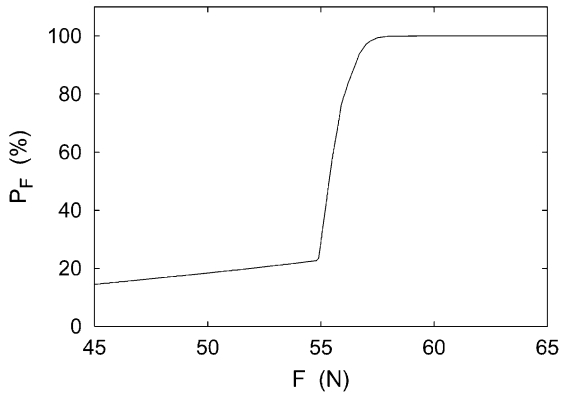

Fig. 8. Probability of edge crack initiation.

of about 55 N, a steep increase occurs, after which the probability very fast approaches its final value.

The local risk (27) in terms of the radial distance to the contact center is shown in Fig. 9. Three loading cases close to the critical load of 55 N are considered. It is found that for small loadings a sharp single peak appears just around the contact boundary r_c. When loading increases, this peak decreases. Instead, a second peak, wider than the first one, appears somewhat in front of the contact boundary. The difference in size of the first and second peak becomes larger with increasing load. It can be concluded that for small loadings crack growth probably occurs directly at the contact boundary, but for higher loadings in front of it.

A comparison with the evolution of the probability (Fig. 8) reveals that the critical load of about 55 N is correlated to the sudden appearance of the second peak in the local risk. This means that crack growth in front of the contact boundary is most responsible for the failure.

The distribution of the local risk of fracture can be understood by studying the stress intensity factors. In Fig. 10, two K-factors for tangentially oriented edge cracks are shown, assigned to a loading of 57 N. Curve (a) is related to cracks located just in front of the second peak in the local risk, curve (b) is related to cracks

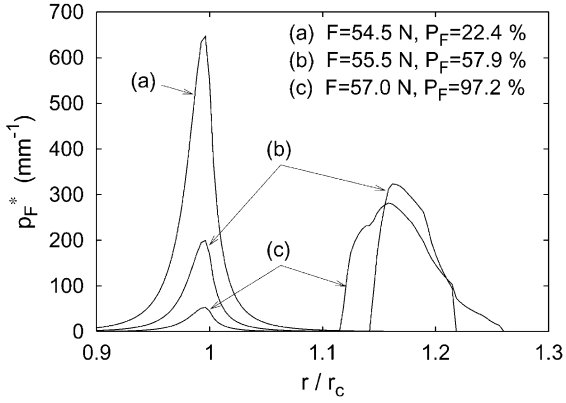

Fig. 9. Local risk of edge crack initiation for different loadings.

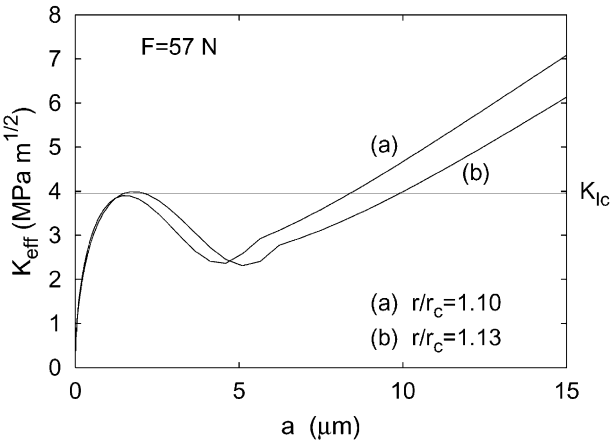

Fig. 10. Stress intensity factor for tangentially oriented edge cracks.

located inside of it. Both K-curves are quite similar, their difference, however, consists in the number of intersection points with the fracture toughness K_{Ic}. The K-curve (a) has only one intersection point at about 8 µm, so that all related cracks which are longer will grow. The contribution of these cracks to the failure probability (24) is small and, therefore, the local risk remains negligibly small at this location. The K-curve (b) has one intersection point at about 10 µm. However, for very small crack lengths, two intersection points occur in addition. Hence, critical cracks exist, which will highly contribute to the failure probability due to their small lengths. This explains the related increase of the local risk.

A survey of the critical crack lengths for tangentially oriented cracks is given in Fig. 11. The curves represent the crack lengths a_i, for which the K-factor equals the fracture toughness, $K_{eff}(a_i) = K_{Ic}$, at the particular radial locations of the cracks. The vertical arrows mark the path of the two related K-curves shown in Fig. 10. The solid lines border the range of critical crack lengths. We see that not only crack lengths above the upper line are critical, but also crack lengths inside the 'elliptical bubble'.

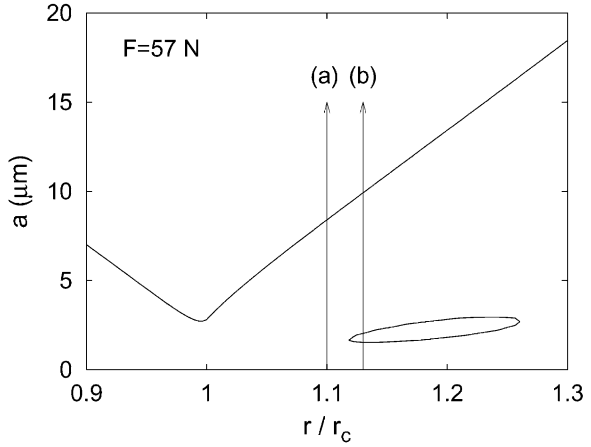

Fig. 11. Border of the range of critical crack lengths for tangentially oriented cracks.

The main contribution to the failure probability is caused by small critical cracks. Such cracks are found around the contact boundary at the lowest point of the upper curve in Fig. 11 and in the region in front of the contact boundary, indicated by the 'elliptical bubble'. This spatial partitioning exactly reflects the distribution of the local risk.

8. Conclusions

Propagation of pre-existing cracks in the strongly non-homogeneous stress field of a sphere indentation test was studied by using a modified Weibull analysis. The main results were:

- A modification of the conventional Weibull theory is proposed which allows the computation of failure probabilities even under steep stress profiles. The method was illustrated for the case of a sphere contact loading test.
- With the computation of the local failure risk, the location of the cone crack initiation could be predicted. For the special choice of material parameters, two possible locations of cone crack initiation were found, one corresponding to the Hertzian contact radius and a second one having a 15% larger radius.
- The total failure probability that increases strongly at a certain load (here at 55 N) provides the load at cone crack initiation.

Acknowledgements

The authors acknowledge the financial support provided by the Deutsche Forschungsgemeinschaft DFG. The work is part of the SFB 483 'High-performance sliding and friction systems based on advanced ceramics'.

References

1. Weibull, W., *A Statistical Theory of the Strength of Materials, vol. 151*. Ingeniorsvetenskaps-akademiens Handlingar, Stockholm, 1939.
2. Batdorf, S. B. and Crose, J. G., A statistical theory or the fracture of brittle structures subjected to nonuniform stress. *J. Appl. Mech*., 1974, **41**, 459–461.
3. Batdorf, S. B. and Heinisch, H. L., Weakest link theory reformulated or arbitrary fracture criterion. *J. Am. Ceram. Soc*., 1978, **61**, 355–358.
4. Evans, A. G., A general approach or the statistical analysis of multiaxial fracture. *J. Am. Ceram. Soc*., 1978, **61**, 302–308.
5. Matsuo, Y., A probabilistic analysis of fracture loci under biaxial stress state. *Bull. JSME*, 1981, **24**, 290–294.
6. Gyekenyesi, J. P. and Nemeth, N., Surface flaw reliability analysis of ceramic components with the SCARE finite element postprocessor program. *Trans. ASME, J. Engng. Gas Turbines and Powers*, 1987, **109**, 247–281.
7. Heger, A., Brückner-Foit, A. and Munz, D., *STAU—ein Programm zur Berechnung der Ausfallwahrscheinlichkeit mehrachsig beanspruchter keramischer Komponenten als Post-Prozessor für Finite-Elemente-Programme*. University of Karlsruhe, Germany, 1991.
8. Lemon, J., Statistical approaches to failure of ceramics reliability assessment. *J. Am. Ceram. Soc*., 1988, **71**, 106–112.
9. Danzer, R., A general strength distribution function for brittle materials. *J. Europ. Ceram. Soc*., 1992, **10**, 461.
10. Danzer, R. and Lube, T., New fracture statistics or brittle materials. *Fracture Mechanics of Ceramics*, 1996, **11**, 425–439.
11. Thiemeier, T., Brückner-Foit, A. and Kölker, H., Influence of the fracture criterion on the failure prediction of ceramics loaded in biaxial flexure. *J. Am. Ceram. Soc*., 1991, **74**, 48–52.
12. Brückner-Foit, A., Heger, A. and Munz, D., On the contribution of notches to the failure probability of ceramic components. *J. Europ. Ceram. Soc*., 1996, **16**, 1027–1034.
13. Hertel, D., Fett, T. and Munz, D., Strength predictions or notched alumina specimens. *J. Europ. Ceram. Soc*., 1998, **18**, 329–338.
14. Brückner-Foit, A., Hülsmeier, P., Sckuhr, M. and Riesch-Oppermann, H. Limitations of the Weibull theory in stress fields with pronounced stress gradients. In *Internat. Gas Turbine and Aeroengine Congress and Exhibition*, Munchen, 8–11 May, 2000. ASME, New York (2000-GT-663).
15. Brückner-Foit, A., Diegele, E., Hülsmeier P., Rettig, U. and Hohmann, C. Prediction of the failure probability of high strength ceramics subject to thermal shock loading. In: *Proceedings of the 26th Annual International Conference on Advanced Ceramics and Composites*, Cocoa Beach, 13–18 January 2002.
16. Fett, T. and Munz, D., Influence of stress gradients on failure in contact strength tests with cylinder loading. *Engng. Fract. Mech*., 2002, **69**, 1353–1361.
17. Fett, T., Ernst, E., Munz, D., Badenheim, D. and Oberacker, R., Effect of multiaxiality and stress gradients on failure in cylinder contact strength tests. *J. Europ. Ceram. Soc*., 2003, **23**, 2031–2037.
18. Alpa, G., On a statistical approach to brittle rupture or multiaxial states of stress. *Engng. Fract. Mech*., 1984, **19**, 881–901.
19. Lawn, B. R., *Fracture of Brittle Solids*. Cambridge University Press, Cambridge, 1993.
20. Lawn, B. R., Indentation o ceramics with spheres: a century after Hertz. *J. Am. Ceram. Soc*., 1998, **81**, 1977–1994.
21. Johnson, K. L., *Contact Mechanics*. Cambridge University Press, Cambridge, 1985.
22. Sackfield, A. and Hills, D. A., Some useful results in the classical Hertz contact problem. *J. Strain Analysis*, 1983, **18**, 101–105.
23. Sackfield, A. and Hills, D. A., Some useful results in the tangentially loaded Hertzian contact problem. *J. Strain Analysis*, 1983, **18**, 107–110.
24. Hertz, H., Über die Berührung fester elastischer Körper. *J. Reine Angew. Math*, 1882, **92**, 156–171.
25. Fett, T. and Munz, D., *Stress Intensity Factors and Weight Functions*. Computational Mechanics Publications, Southampton, 1997.
26. Fett, T. and Munz, D., Kinked cracks and Richard Fracture criterion. *Int. J. Fracture*, 2002, **115**, L69–L73.
27. Fischer-Cripps, A. C., Predicting Hertzian fracture. *J. Mater. Sci*., 1997, **32**, 1277–1285.
28. Kocer, C. and Collins, R. E., Measurement of very slow crack growth in glass. *J. Am. Ceram. Soc*., 2001, **84**, 2585–2593.
29. Fett, T., Effective Mode-II Stress Intensity Factor for Partially Opened Natural Cracks under Mixed-mode Loading. Presented at the ICF10,Honolulu, Dec. 2001.
30. Fett, T., Mixed-mode stress intensity factors or partially opened cracks. *Int. J. Fract*., 2001, **111**, L67–L72.